Variable angle photoelectron spectrometer*

Douglas C. Mason, Donald M. Mintz,† and Aron Kuppermann

Arthur Amos Noyes Laboratory of Chemical Physics,‡ California Institute of Technology, Pasadena, California 91125

(Received 22 September 1975; in final form, 17 June 1976)

The design, construction, and performance of a spectrometer for measuring the angular and energy distributions of electrons photoejected by rare gas resonance light is described. Results using 584.4-Å photons from a helium lamp are reported. Flexibility of instrumental design allows for the use of other light sources. A 180° hemispherical electrostatic electron energy analyzer is rotatable about the center of an enclosed sample chamber. The instrument is highly automated, with an on-line computer used to control the detector angle and the data acquisition and reduction. This automation is required by the long and continuous data acquisition.

I. INTRODUCTION

Since the early 1960s, photoelectron spectroscopy has found wide acceptance as a tool for studying the electronic structure of molecules.[1,2] Monochromatic light sufficiently energetic to ionize atoms or molecules ejects photoelectrons whose energies are given by

$$E_e = h\nu - E_I,$$

where E_I is the energy needed to ionize the molecule. The resulting ion can be electronically, vibrationally, and rotationally excited. E_I is determined from a knowledge of $h\nu$ and measurement of E_e and furnishes information on the strength of molecular bonds, molecular geometry in ground and ionic states, and intramolecular interaction of functional groups.[2] In addition, the measurement of photoelectron intensities as a function of photon energy has facilitated the modeling of complex processes in plasmas and in the upper atmosphere.[3]

Since 1968,[4,5] it has been realized that the angular distribution of photoelectrons contained additional information of value in the interpretation of their energy spectra. Briefly, for nonpolarized light, the angular distribution for electric-dipole ionization has the form

$$\frac{d\sigma}{d\Omega} = \frac{Q}{4\pi}\left[1 - \tfrac{1}{4}\beta(3\cos^2\theta - 1)\right], \qquad (1)$$

where $d\sigma/d\Omega$ is the differential photoelectron cross section for a given transition, Q is the corresponding total cross section, θ is the angle between the light axis and the velocity vector of the outgoing electron, and β is a single asymmetry parameter in the range -1 to 2 that describes the deviation of the angular distribution from an isotropic one. The values of β and Q depend on the characteristics of the electron ejected, such as its angular momentum, and on the wavelength of the light employed.

The first modern experimental work in measuring photoelectron angular distributions was carried out by Berkowitz and Ehrhardt,[6] who employed a moveable electrostatic retarding grid energy analyzer and a fixed lamp. More recent approaches to measuring photoelectron angular distributions using vacuum ultraviolet excitation can be divided into four categories.

Carlson,[7] following on the success of employing moveable x-ray sources for measuring x-ray photoelectron angular distributions, has rotated the lamp around a fixed ionization region followed by a stationary energy analyzer. Results have been obtained in studies of a wide range of sample vapors.[8] In this arrangement, relatively simple lamps can be used; variation of incident wavelength using a rotatable monochromator and continuum light source would be very cumbersome. In a similar spirit, the angular distributions of photodetached electrons have been studied by rotating the polarization direction of a laser light source.[5]

A second group has employed two separate light sources of different degrees of polarization.[9,10] Here, both the lamp and detector are fixed and β may be extracted[11] from a knowledge of photon polarization and relative intensity in the two experiments. This method suffers from a lack of measurement redundancy and consequently, the presence of experimental artifacts that affect the angular distribution and yield spurious results cannot be detected directly.

Several groups have opted for a multiple detector for measuring photoelectron angular distributions. Ames *et al.*[12] and Samson[13] have used a pair of Channeltron-type electron multipliers accepting electrons emerging from a single energy analyzer after having been ejected in different directions from a single ionization region. These measurements suffer principally from lack of redundancy and the need to normalize results to β values obtained by other methods. Both experiments assume that relative detector response is constant with time. Early results obtained by McGowan *et al.*[14] used a sectored spherical retarding potential analyzer. In order to maximize signal into an electrometer, large sectors subtending a 15° range in θ were employed. Angular resolution is thus 15° and the effect of averaging the angular distribution over θ must be considered. The inability to operate the detector in a pulse-counting mode limits

 Copyright © 1977 American Institute of Physics

Downloaded 21 Dec 2005 to 131.215.225.171. Redistribution subject to AIP license or copyright, see http://rsi.aip.org/rsi/copyright.jsp

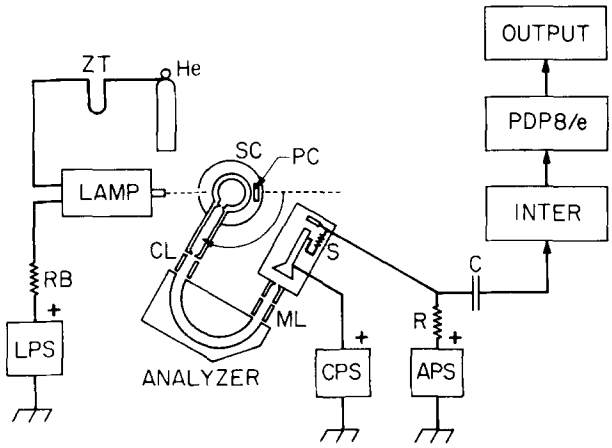

FIG. 1. Block diagram of variable angle photoelectron spectrometer. He—cylinder of UHP helium; ZT—liquid nitrogen immersed Zeolite trap for lamp helium supply; RB—lamp ballast resistor, 1320 Ω; LPS—lamp power supply, 555 V, 300 mA maximum; SC—sample chamber; PC—photocathode for light flux measurement; CL—electron lens elements before hemispherical analyzer; ANALYZER—180° hemispherical electrostatic electron energy analyzer; ML—electron lens elements between hemispheres and detector; S—Spiraltron electron multiplier; CPS—power supply to Spiraltron cathode; APS—power supply to Spiraltron anode; *R*,*C*—differentiating network for Spiraltron pulses, $R = 1$ MΩ, $C = 500$ pF; PDP8/e—Digital Equipment Corporation minicomputer; INTER—counting system interface to experiment; OUTPUT—computer output devices to user.

experimental sensitivity. Results for low electron energies (Ne I ionization of Ar) indicated artifacts due to stray electric or magnetic fields.

A fourth approach, the one originally employed by Berkowitz and Ehrhardt,[6] uses a stationary line source lamp and a single moveable detector. This has been the method favored subsequently by Morgenstern *et al.*,[15] Harrison,[16] Dehmer *et al.*,[17] and the present workers.[18] Flexibility in choice of light source is one consequence of this design approach.

Several recent studies with tunable light sources and moveable electron energy analyzers appear promising. Houlgate *et al.*[19] and Watson and Stewart[20] have measured photoelectron angular distributions for noble gases using synchrotron radiation and a vacuum ultraviolet monochromator. When the experimental arrangement is fully optimized to permit them to obtain spectra at high resolution[21] this should be a very powerful technique for the study of molecular photoionization.

II. APPARATUS

A block diagram of the apparatus is given in Fig. 1. It consists of a lamp, a sample chamber, and an energy analyzer, all mounted on an 46-cm-diam stainless steel flange which is bolted to a high vacuum system, and a data acquisition system. The individual components are described below.

A. Lamp

The He I (584.4 Å) capillary discharge lamp is a variant of the Geissler tube described by Newburgh *et al.*[22] A scaled section view is given in Fig. 2. Matheson UHP grade helium flows through a Linde-type 4X molecular sieve-filled trap immersed in liquid nitrogen before entering the rear of the lamp. The discharge is maintained between a low magnetic permeability stainless steel anode at positive high voltage and a grounded tungsten carbide cathode through a quartz capillary of length 19 mm and bore 2 mm. Other materials used in fabricating the lamp include aluminum for the main body, boron nitride for insulators, and elastomeric O-ring seals that allow the lamp to be tested outside of the vacuum chamber.

The region between discharge and the main vacuum chamber is pumped by a ½-liter/sec and a 2½-liter/sec mechanical pump in a differential pumping arrangement. This reduces the pressure rise in the main vacuum chamber to 10^{-5} Torr during lamp operation. Light passes through a 0.9-mm-diam aluminum capillary before entering the sample chamber. Kerosene lines connected to a recirculating pump and heat exchanger cool the lamp during operation. Lamp power is supplied by a Fluke model 407 power supply through a 1320-Ω, 150-W ballast resistor. The discharge is initiated by striking a Tesla coil to a starter electrode located in back of the anode.

The lamp cathode was ground from tungsten carbide in order to maximize resistance to cathodic sputtering. Sputtering over a period of two months of continuous lamp operation constricts the light exit hole in the cathode by (20–30)%. Previous designs employing molybdenum cathodes underwent degradation of similar magnitudes in operation periods of only two weeks.

Typical lamp operating parameters are a discharge current of 100 mA and an anode voltage of +365 V. Precise measurements of operating pressure inside the lamp are not made. However, between the molecular

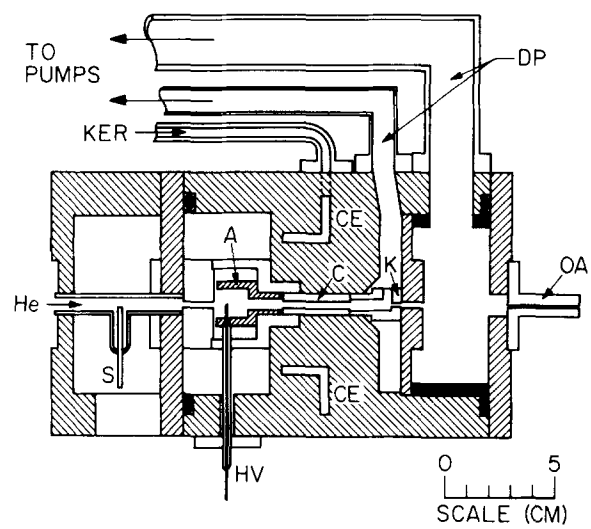

FIG. 2. Section view of lamp. Hatched and stippled parts, except for the stainless steel lamp anode, A, are of aluminum and constitute the lamp body. K—tungsten carbide cathode; C—quartz discharge capillary; HV—high voltage power lead; S—starter electrode; He—helium inlet; OA—lamp flux outlet capillary; DP—differential pumping connections; KER—kerosene cooling inlet (outlet not shown); CE—kerosene cooling envelope inside lamp body. Flows of helium and kerosene are indicated by horizontal arrows.

Downloaded 21 Dec 2005 to 131.215.225.171. Redistribution subject to AIP license or copyright, see http://rsi.aip.org/rsi/copyright.jsp

sieve trap and the lamp body, a Wallace and Tiernan manometer registers 8 Torr, so that the lamp operating pressure is estimated at 2–4 Torr.

Photon flux is monitored inside the sample chamber by a photodiode similar in design to that of Samson.[23] The anode of the flux-measuring device, at a potential of +12 V, is hidden from the inside of the sample chamber by a strip of 40 lines/cm gold mesh which is maintained at the same potential as the tungsten photocathode. A Victoreen model VTE-2 electrometer measures the photocathode current to ground. Assuming a 14% quantum efficiency of the undegassed photocathode surface,[24] we estimate a photon flux of 1.8×10^{11} photons/sec passing through the ionization region. The angular width of the light beam, as determined by appropriate apertures, was 1.8°.

The lamp was tested on a vacuum ultraviolet monochromator without Zeolite trapping on the helium. Only one significant vacuum ultraviolet impurity line at 1216 Å was observed, but its intensity did not exceed 1% of the 584.4 Å principal line. Subsequent tests on the photoelectron spectrometer run with CS_2 in the sample chamber, as recommended by Turner,[2] revealed no detectable low electron energy peak arising from 1216-Å ionization to the $\tilde{X}$ ionic state.

Lamp parameters of helium pressure and discharge current are adjusted to maximize the photocathode current. Under these conditions, photoelectrons arising from ionization by the helium 537-Å ($1s^2 \leftarrow 1s3p$) and 522-Å ($1s^2 \leftarrow 1s4p$) lines are observed with respective counting rates of 2 and 0.5% of the corresponding 584.4-Å peaks.

B. Sample chamber

The sample chamber was designed to maximize electrostatic shielding, minimize gas leakage, and reduce the photoelectron background counting rate produced by the unabsorbed photon beam. The sample chamber, shown in Fig. 3, consists of three coaxial shells made of gold-plated copper. Gas enters the base through GI into the inner chamber, IS. Electrically, this chamber is insulated from the other chambers and is connected to the rotating energy analyzer. The middle shell, MS, remains fixed with respect to the lamp. The photon beam enters the inner shell by a slot, HS, in the outer shell, OS, a 2-mm aperture, LI, in the middle shell, MS, and a slit in the inner shell. The unabsorbed photon beam is trapped at the photocathode assembly mounted on the middle shell (not shown in Fig. 3) after passing completely through the inner shell. As the observation angle is changed, the outer shell rotates with the detector and undergoes translation along the chamber axis, guided by the helical slot, HS, and guide screw, GS. Thus, the light entrance hole is not obscured. The outer sleeve incorporates Teflon gaskets to the middle shell in order to minimize gas leakage. Mechanical interactions inside the sample chamber limit the range of permissible detector angles to 38°–126° with respect to the light axis.

Gas samples are manipulated on a small glass inlet

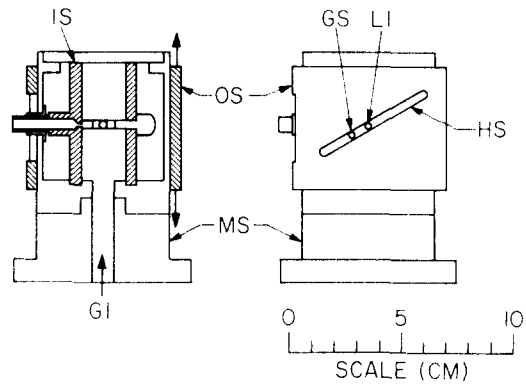

FIG. 3. Section and external views of sample chamber. Hatched areas are sections of the inner and outer shells. OS—outer shell; MS—middle shell; IS—inner shell; GI—gas inlet; HS—helical slot; GS—guide screw for helical slot; LI—light inlet hole. Motion of OS and flow sample are shown with vertical arrows.

manifold before they are introduced into the instrument. In order that the sample chamber pressure change only slowly with time, the sample gas is stored in a 5-liter ballast bulb during operation. The samples are admitted into the sample chamber through a Granville Phillips model 203 variable leak valve. When samples are liquids at room temperature, we do not use the ballast, but instead admit the vapor directly from the bulb containing the sample. The leak valve is in this case heated to 40 °C to prevent condensation at the valve orifice and the accompanying irregularity of flow. In order to avoid cross contamination of one sample by preceding ones, the glass manifold is baked in an annealing oven when changing from one substance to another.

Sample gases enter the sample chamber through the base of the middle shell. A duct connected to that base leads to a Westinghouse-type WL-7903 high pressure ionization gauge mounted outside of the vacuum chamber on the 46-cm main flange. The gauge output signal varies linearly with pressure in our normal range of operating pressures of 2–5 mTorr.

We have found that sulfur and halogen-containing organics damage the high pressure ionization gauge filament for sample pressures in the range 2–4 mTorr. A capacitance manometer would be a better, albeit a more expensive, sample pressure measuring device.

Detected photoelectron signal I_{pe} depends on sample pressure via a Lambert-Beer law:

$$I_{pe} = AI_{ph}[1 - \exp(Q_{pe} n l_{pe})] \exp(-Q_{es} n l_{es}), \quad (2)$$

where I_{ph} is the initial photon flux, Q_{pe} and Q_{es} are the total cross sections for photoionization and electron scattering, respectively, and l_{pe} and l_{es} are the pathlengths over which photoionization contributes to detected signal and electron scattering attenuates it, respectively. A is an overall detection efficiency constant. The number density of absorbers or scatterers n is proportional to pressure. The total electron scattering cross section is several orders of magnitude larger than the photoionization cross section for the typical range of electron and photon energies encountered in this experiment. As a result, a nonlinear dependence of I_{pe} on

Downloaded 21 Dec 2005 to 131.215.225.171. Redistribution subject to AIP license or copyright, see http://rsi.aip.org/rsi/copyright.jsp

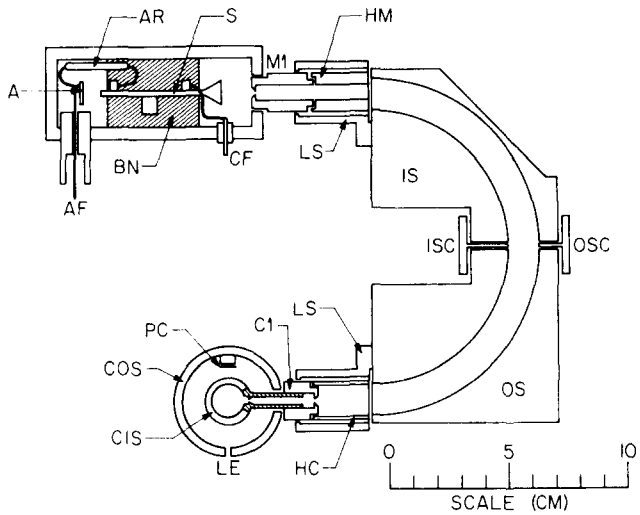

FIG. 4. Section view of electron analyzer and sample chamber in plane of electron trajectories. Hatched areas include BN, a boron nitride mounting block for S, the Spiraltron, and part of CIS, the inner shell of the sample chamber. COS—outer shell of sample chamber; PC—photocathode; LE—light entrance; C1, HC, HM, and M1—lens elements; LS—aluminum supports for lens elements; IS—inner hemisphere; OS—outer hemisphere; ISC—corrector to inner hemisphere; OSC—corrector to outer hemisphere; AL—aluminum enclosure for Spiraltron; CF, AF—electrical feedthroughs for Spiraltron; AR—resistor from Spiraltron anode to anode plate A.

pressure can arise from electron scattering even at pressures sufficiently low for the term $1 - \exp(Q_{pe} n l_{pe})$ to be a linear function of pressure. In order to maximize the signal to background ratio, we operate at the maximum pressure for which the photoelectron counting rate depends linearly on pressure. The maximum pressure is determined separately for each substance studied. Typical maximum permissible operating pressures are 4 mTorr for nitrogen and argon.

C. Electron energy analyzer and detector

The electron energy dispersion and detection system is composed of four parts: a decelerating lens, a 180° double focusing hemispherical analyzer,[25] an accelerating lens, and a Spiraltron electron multiplier. The whole detection system is mounted on a single 200-mm-diam worm gear and is rotated about the (horizontal) axis of the sample chamber. This gear must be lubricated periodically with molybdenum disulfide to limit wear. The lens elements and hemispheres were fabricated from OFHC grade copper and plated with 24K gold. The lenses are held rigidly in place by boron nitride spacers and aluminum mounting brackets bolted directly to the inner hemisphere. A scaled section view is shown in Fig. 4.

Apertures of 1.0-mm diameter in the inner shell of the sample chamber and the first lens element limit the detector acceptance half angle to 2.1°. The hemispherical analyzer is operated in the constant electron energy mode[26] in order to optimize electron energy resolution. The lens formed by elements C1 and HC decelerates photoelectrons, initially having kinetic energy T, to a fixed energy V usually chosen to be 1.5 eV. The difference $T - V$ is called the sphere center energy. Spectra are generated by sweeping the potential applied to the lenses HC, HM, and M1 and the various sphere elements with respect to C1, which is connected to the inner shell of the sample chamber. This mode has the advantage that the absolute energy resolution remains roughly constant over the full range of the spectrum. This resolution, measured at the full width at half maximum (FWHM) of the $^2P_{3/2}$ peak obtained from the ionization of Ar by 736 and 584 Å and obtained from the ionization of Xe by 584-Å light, was not noticeably different. This corresponds to electron energies of 1, 5.5, and 9 eV and deceleration ratios of 0.7, 4, and 6.

The operation of the hemispherical energy analyzer has been discussed at length by Purcell.[25] Our analyzer has a mean radius of 38.1-mm and a 1.27-mm radial gap between inner and outer spheres. Space and weight restrictions have dictated that we not use full hemispheres; the sides were cut off and the hemisphere halves are surrounded by a stainless steel bracket held at the sphere center potential.

We anticipated deviations from the nominal $1/r$ analyzing field because of this modification. As a result, we incorporated correcting electrodes halfway around the hemispheres. Turner[27] has found correcting electrodes like these helpful in improving resolution in 127° cylindrical analyzers. To date the spectrometer has been operated with the inner sphere and outer sphere corrector electrodes left at the potentials of the corresponding spheres. Contamination of the electron energy analyzer surfaces tends to slowly reduce counting rates over periods of a month, requiring periodic cleaning.

After emerging from the analyzer and Herzog element, the photoelectrons are accelerated to 6.5 eV by a final cylindrical lens and focused through a 1.0-mm-diam aperture in the rear of that lens. Thereafter, they are accelerated into the front cone of a Bendix model 4219X Spiraltron electron multiplier biased at +60 V with respect to ground. The Spiraltron is mounted on a boron nitride support by two of its electrical connecting tabs, and is enclosed in an aluminum chamber to eliminate being reached by stray electrons. We operate the Spiraltron as a two-terminal device. Its anode is connected via a 1000-MΩ glass-encapsulated resistor to a copper collector plate and a +3200-V power supply.

Charge pulses at the copper collector are converted into voltage pulses by a differentiating network. The voltage pulses, 10–50 mV in height, are amplified and discriminated by a specially designed pulse amplifier involving inexpensive and easily replaceable components. This facilitates its repair when it is damaged by high voltage breakdowns in the system.

The inner shell of the sample chamber, the Herzog elements, and the hemispheres are coated with Aquadag in order to reduce the probability of reflection of electrons from surfaces. The Aquadag surfaces are polished in order to reduce fluctuations in contact potentials.[28] The spheres and lenses may be baked by heaters mounted on the inner hemisphere. After continuous

Downloaded 21 Dec 2005 to 131.215.225.171. Redistribution subject to AIP license or copyright, see http://rsi.aip.org/rsi/copyright.jsp

operation for about one month in the presence of organic samples the counting rates deteriorated by a factor of 2–3. Baking to approximately 200 °C for 18 h with no sample in the machine usually restored the counting rates to about 80% of their original values.

The sample chamber volume from which photoelectrons are detected varies inversely with the sine of the detector angle θ, providing the lamp and energy analyzer view cones subtend small angles, and that θ is near 90°. For the present view cone geometries, the deviation from the above form is less than 0.2% for θ between 40° and 120°. Thus, if the light beam and the sample chamber gas density are assumed homogeneous, multiplication of peak intensities by $\sin\theta$ should yield good fits of $I(\theta)$ to Eq. (1).

The configuration of sample chamber sliding seals and slots results in a sample pressure which is detector angle dependent. It is approximately 15% lower at 80° than it is at 40° and 120°. Pressure compensation for these large pressure changes becomes a necessity. Since our counting rate dependence on pressure is linear, it is a simple matter to compensate for angular variations of sample pressure.

A schematic of the lens and sphere voltage distribution system is shown in Fig. 5. To take a photoelectron spectrum we step the output voltage of a 12-bit digital-to-analog converter under computer control to give the desired energy increments. Biasing power supplies and operational amplifiers supply voltages to the lens and sphere elements. The use of operational amplifiers reduces output impedance below 1 Ω and the output voltage ripple below 5 mV peak to peak.

A typical spectrum obtained with an analyzing energy of 0.75 eV is shown in Fig. 6. Normally, in order to maximize signal rates and to reduce susceptibility of changing surface conditions, we operate at an analyzing energy of 1.5 eV for which the resolution is about 30 meV. Furthermore, faster electrons are less susceptible to magnetic field deflections and thus angular distributions are less prone to magnetic-field-induced artifacts at this higher analyzing energy.

D. Additional experimental hardware

A Bodine NSH-12R reversible 1/50 horsepower dc motor controls the detector angle. The motor drive shaft is linked to the main worm gear via a stainless steel worm through a rotary motion feedthrough on the instrument main flange. For each revolution of the drive shaft, a detector rotates by 1 deg. The drive shaft is geared to a Disc model 100 incremental shaft encoder which makes ten dry reed switch contacts for each full shaft rotation. The detector angle is determined by counting switch closures from the previous angle and noting the direction of shaft rotation. Under operating conditions, the detector angular position is known to ±0.2°. Internal alignment is assured by appropriately located positioning pins.

To eliminate the earth's magnetic field, the inside of

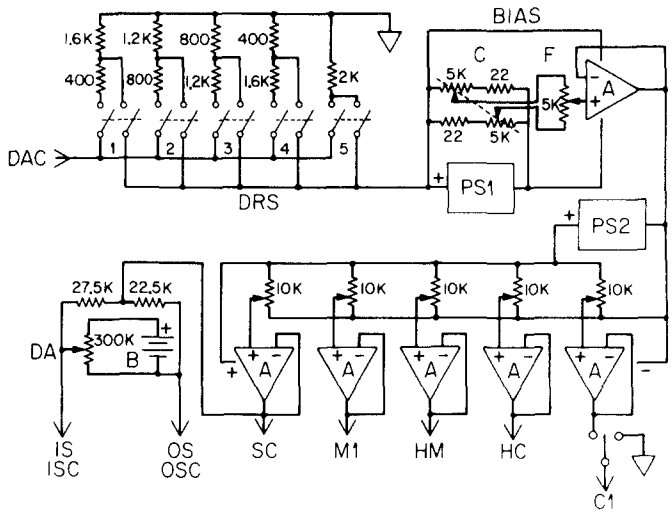

FIG. 5. Circuit schematic of lens and sphere voltage distribution system. Biasing networks for inner and outer sphere correctors, ISC and OSC, are omitted. Resistances are given in ohms; K = times 1000. The amplifiers, A, are Texas Instrument's SN72741. DAC—input from a computer digital-to-analog converter; DRS—select digital resolution, the incremented analog voltage between DAC channels in steps of 1–5 mV; PS1—18-V power supply; BIAS—adjustable bias voltage circuit for all lens elements that varies the accepted electron energy; C—coarse adjustment via tandem potentiometers; F—fine adjustment; PS2—37-V power supply; B—three 1.35-V mercury cells in series; C1, HC, HM, H1—conductors to lens elements; SC—conductor to sphere mounting bracket held at sphere center voltage; IS, OS, ISC, OSC—conductors to sphere elements; DA—user adjustment of IS-OS voltage.

the vacuum chamber is lined with a single layer of 1.27-mm Mu-metal shielding in which holes are provided for the connections to the main diffusion pump and the main flange. The resulting magnetic field in the region traversed by the electrons is about 10 mG.

Owing to the motion of the detector, the residual magnetic field caused spurious asymmetries in the angular distribution. To eliminate these asymmetries, the main vacuum chamber was surrounded by three pairs of square Helmholtz coils whose sides measure about 3 m in length. The east–west and north–south coils are separated by the recommended distance,[29] 0.544 times the edge length, which minimizes field gradients between the coils along their axes. The vertical pair lie on the floor and above the E–W and N–S pairs in order to facilitate access to the vacuum chamber.

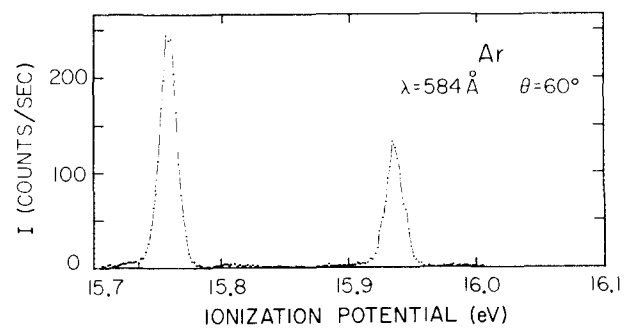

FIG. 6. High resolution He I spectrum of argon $^2P_{3/2}$ (left) and $^2P_{1/2}$ at $\theta = 60°$. The spectrum was taken at an analyzing energy of 0.75-eV and at 2-meV electron energy increments between successive channels. Resolution for the $^2P_{3/2}$ peak is 16-meV FWHM.

Downloaded 21 Dec 2005 to 131.215.225.171. Redistribution subject to AIP license or copyright, see http://rsi.aip.org/rsi/copyright.jsp

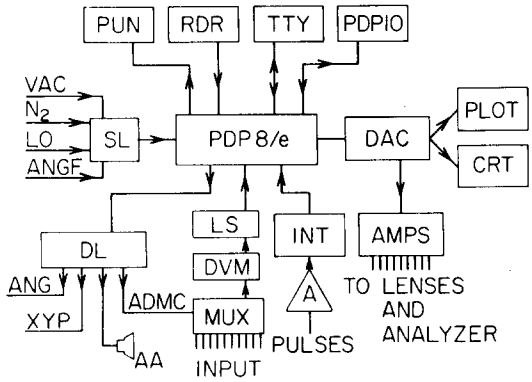

FIG. 7. Block diagram of computer-based data acquisition system. Direction of flow of information is indicated by arrows. PDP8/e—minicomputer; PUN, RDR—high speed paper tape punch and reader; TTY—Teletype ASR33 terminal; PDP10—interface to PDP10; DAC—three-channel digital-to-analog converter; PLOT—X,Y plotter; CRT—cathode ray tube for display of spectra; AMPS—amplifiers for lens and sphere voltage control; INT—counting interface, including counter and digital display; A—Spiraltron pulse amplifier; INPUT—input for ten analog voltages from lenses, etc; MUX—dual ten-channel analog multiplexer; DVM—autoranging voltmeter; LS—logic signal level shifter; DL—drive line interface between instrument and computer; ANG—signal to angle drive for increasing or decreasing θ; XYP—signal to X,Y plotter to lower pen; AA—signal to audio alarm; ADMC—signal to place multiplexer under computer control; SL—sense line interface between instrument and computer; ANGF—angle drive feedback; LO—lamp status signal; N_2—liquid nitrogen baffle-filling status signal; VAC—vacuum system status signal.

The coils were constructed from 40 km of 26 AWG copper magnet wire wound around aluminum foil forms. This brings the residual magnetic field down to 0.3 mG and makes detection efficiency independent of detector angle.

Several times after line voltage power failures, some lasting only a fraction of a second, we found the need to perform extensive degaussing of instrument parts made of 304 stainless steel and of the Mu-metal shield. The magnetic field transients resulting from transients in the primary power to the three dc regulated Helmholtz coil power supplies induced permanent magnetism in susceptible metals. The solution to this difficulty was to install a Topaz model 315-BK-12 uninterruptible power supply rated at 300 VA maximum inverter capacity. The switching times of 10–15 msec of this device were found not to magnetize the instrument components. A 90-Ah lead–acid battery provides backup power for as long as 1 h in the event of a power failure.

The main vacuum chamber is pumped by a Varian-NRC model VHS-6 oil diffusion pump trapped with a Varian-NRC 15-cm liquid-nitrogen-cooled baffle. The outlet side of the main diffusion pump is backed by a CVC model MCF 300 oil diffusion pump which acts as a booster stage. The two diffusion pumps are separated by a Freon-cooled chevron baffle. Between the diffusion pumps and a rotary mechanical pump is a molecular sieve trap to limit mechanical pump oil contamination of the diffusion pump oil.

We reach a base pressure of 2×10^{-7} Torr after a day of pumping. Total sample and helium background pressures in the main chamber during operation is typically 1.5×10^{-5} Torr.

E. Data acquisition system

1. Hardware

Low photoelectron counting rates for most of the samples studied require long data acquisition times. It was necessary to record sample chamber pressure, lamp flux, and other experimental parameters over the 1–9 h interval of a typical angular distribution. Some on-line data reduction, the location and counting rates at photoelectron peaks, as well as a paper tape record of each spectrum, were desirable in order to save data for later manipulation. The need to provide redundancy in measuring the angular distribution parameter β by a fit to intensities at more than two angles has been discussed above. In order to free us from physical presence in the lab to change the detector angle for each successive spectrum, automatic control of the angle drive system was desirable.

We found a computer-based data acquisition system ideally suited to these measurement and control functions over long periods of time. A block diagram of this data acquisition system is given in Fig. 7.

A Digital Equipment Corporation model PDP8/e minicomputer forms the heart of the data acquisition system. Standard computer peripheral devices include a Teletype terminal (TTY), a photoelectric paper tape reader (RDR), a high speed paper tape punch (PUN), and an interface to a computer on the Caltech campus (PDP10).

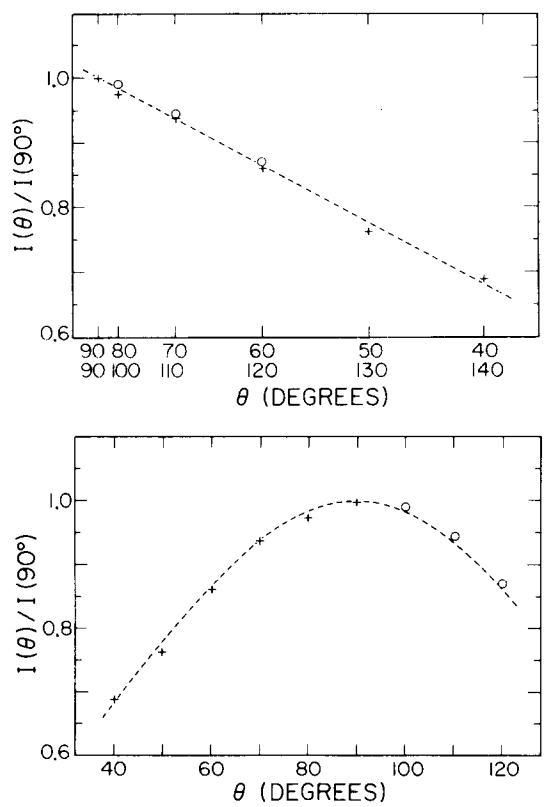

FIG. 8. Signal intensity, corrected for angle-dependent scattering volume and pressure, and normalized to unity at 90°, as a function of scattering angle θ. For the upper figure the abscissa is $\cos^2\theta$ and for the lower one, θ. The circles indicate points for $\theta > 90°$ and the crosses $\theta \leq 90°$. The dashed curves represent the least squares fit ($\beta = 0.88$) to these points according to Eq. (1).

Downloaded 21 Dec 2005 to 131.215.225.171. Redistribution subject to AIP license or copyright, see http://rsi.aip.org/rsi/copyright.jsp

TABLE I. Values of β for ionization of argon by He I light.

$^2P_{3/2}$	$^2P_{1/2}$	Source
0.88 ± 0.02	0.86 ± 0.02	Present work
0.85 ± 0.05	0.85 ± 0.05	Carlson *et al.*[a]
0.95 ± 0.02	0.95 ± 0.02	Morgenstern *et al.*[b]
0.9		McGowan *et al.*[c]
0.4		Berkowitz *et al.*[d]
0.3		Sampson[e]
0.90_5	0.88	Hartree–Fock dipole length Kennedy and Manson[f]
0.88	0.85_5	Hartree–Fock dipole velocity[f]

[a] Reference 7. [d] Reference 6.
[b] Reference 15. [e] Reference 13.
[c] Reference 14. [f] Reference 33.

Other standard hardware features include a real time clock and three channels of digital-to-analog conversion (DAC). The real time clock supplies a 120-Hz time base for measuring counting rates. One digital-to-analog converter channel operates the energy scanning electronics actively. Two digital to analog converter channels permit oscilloscope display (CRT) of spectra during data acquisition with counting rate along the Y axis and electron energy along the X axis. These same two digital to analog converters provide plotting capability on an $X-Y$ recorder (PLOT).

2. Data acquisition

From the standpoint of operating software, the 8K words of computer memory are divided into two 4K segments. A systems program in the first 4K of nonvolatile core memory provides access to software floating point routines, photoelectron spectrometer control functions, input–output devices, and the real time clock for higher level user programs in the second 4K of volatile semiconductor memory. To implement this, we operate the second 4K in a time-sharing mode. Linkage to system routines from data acquisition and reduction programs is provided by pseudoinstructions which interrupt the processor (computer trap).

Data-taking software allows the PDP8/e to take data in the manner of a multichannel scaler. Several features of the computer-based system provide important flexibility. The user can select from 1 to 511 data-taking channels, where each channel has the capacity of over 8 million counts. This flexibility allows us to scan different kinds of spectrum features with different numbers of channels. At the conclusion of each single pass over the full spectrum, the computer measures the sample pressure. After the last pass, an average pressure obtained from dividing the sum of all pressure readings by the number of readings is automatically printed on the Teletype console. This feature allows one to compensate partially for pressure changes.

In the normal mode of taking angular distributions, we measure spectra at detector angles varying from 40° to 120° in 10° increments. An experimental counting rate background of 0–2 counts/sec rises toward low electron energy but is independent of sample pressure. We measure background spectra at each of the nine detector angles just mentioned and parameterize the results as a series of three line segments. Subsequent calculation of β is made correcting this background.

3. Data reduction

Computational capabilities of the computer-based data acquisition system allow for partial on-line reduction of the raw data. Spectra are smoothed by the least squares method of Savitzky and Golay.[30] A routine based upon the Savitzky and Golay least squares derivative algorithm[30] then locates the peak maxima.

We obtain values of β from the angular dependence of pressure compensated, volume corrected counting rates by a weighted least squares fit to the expression

$$I(\theta) = A + B \sin^2\theta. \tag{3}$$

The linear parameters A and B are determined by simple linear regression theory.[31] Weights are chosen inversely proportional to the variance in the measurement of counting rate (which is equal to the number of counts) and are normalized to nine, the number of values of θ used. The variance σ_β^2 of β is obtained from propagating the variances σ_A^2 and σ_B^2 of[32] A and B:

$$\sigma_\beta^2 = \left(\frac{\partial\beta}{\partial A}\right)^2 \sigma_A^2 + \left(\frac{\partial\beta}{\partial B}\right)^2 \sigma_B^2. \tag{4}$$

Here σ_A^2 and σ_B^2 are obtained from diagonal elements of the weighted least squares variance-covariance matrix.[31] The lengths of the error bars in the β curve of Fig. 9 are equal to σ_β. A PDP8/e 8K system-based program performs the calculation of β just described.

III. RESULTS

Figure 8 shows an angular distribution for the Ar^+ $^2P_{3/2}$ peak. The peak intensity has been pressure com-

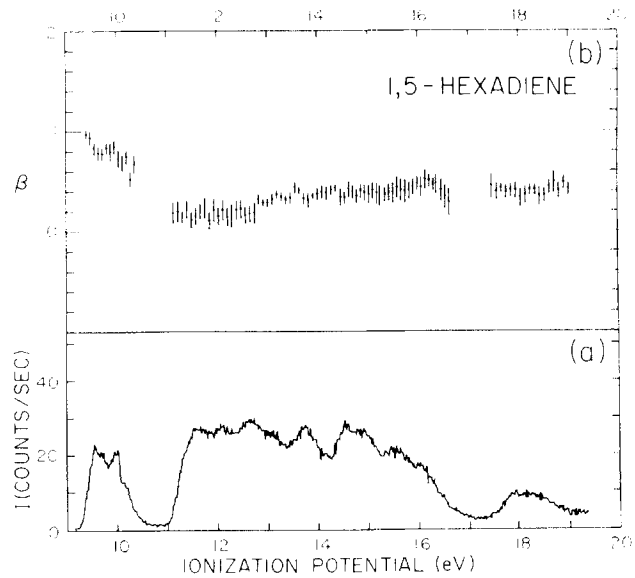

FIG. 9. (a) He I photoelectron spectrum of 1,5-hexadiene at $\theta = 54.7°$ in lower frame. The spectrum was taken over 511 data channels with a difference of 20 meV between the electron energies for successive data channels. (b) Variation of β with ionization potential.

Downloaded 21 Dec 2005 to 131.215.225.171. Redistribution subject to AIP license or copyright, see http://rsi.aip.org/rsi/copyright.jsp

pensated, volume corrected, and divided by pressure compensated intensity at $\theta = 90°$. The dashed curves correspond to the least squares fit which yields $\beta = 0.88$, and as can be seen, its fit to the experimental points is very satisfactory. The value of σ_β is 0.02.

Our results for argon ionized by the He I line are presented in Table I together with those of other workers and theoretical calculations. We observe a slight difference between the $J = 3/2$ and $J = 1/2$ spin-orbit components that is in good agreement with calculations of Kennedy and Manson.[33] Carlson *et al.*[7] and Morgenstern *et al.*[15] have observed similar behavior in He I ionization of xenon and krypton, where the difference in β for the two spin-orbit components is appreciably larger.

In Fig. 9 we display the results for a large polyatomic molecule, 1,5-hexadiene, run with the present apparatus. This substance was obtained from the Aldrich Chemical Co. It had a stated purity of 98% and was used without further purification. The sample was degassed by several freeze, pump, thaw cycles on our sample inlet manifold using liquid nitrogen as the cooling agent. Measurement of all the indicated photoelectron angular distributions required three days. The full spectrum was divided into five segments of width approximately 1.5 eV and a nine-angle angular distribution of each segment required 9–10 h. This spectrum was energy-calibrated by taking a spectrum of mixture of 1,5-hexadiene with argon.

Previous measurements of photoelectron angular distributions for a series of acyclic olefins have shown that β values for π electrons ejected from C-C double bonds are larger by 0.6–0.9 than for σ electrons ejected from C-C and C-H single bonds,[8,18,34] when the photoelectrons have comparable energies. This finding and the β values of Fig. 9 lead us to assign the 9.2–10.5-eV region as arising from the ionization of C-C double bond π electrons. This use of angular distributions to interpret photoelectron spectra is an indication of the usefulness of these kinds of measurements. We also attribute the diffuse band which covers the ionization energy range from 11–17 eV and the band centered about 18.2 eV to ionization from C-C and C-H σ bonds. The band between 9.2–10.5 eV has two prominent maxima, one at 9.59 eV and the other at 10.01 eV, which have been assigned[35] as π_- and π_+ combinations of the weakly interacting double bonds. A more detailed analysis of this molecule will be published elsewhere.

ACKNOWLEDGMENTS

We wish to express our thanks to the members of the Instrument Shop of the Division of Chemistry and Chemical Engineering for their gifted assistance in the construction of the instrument, with particular thanks to W. Schuelke and A. Stark. We also thank Dr. O. A. Mosher for his participation in the design of the pulse amplifier.

* Work supported in part by a contract with the United States Energy Research and Development Administration. Report Code: CALT-767P4-142.

† Work performed in partial fulfillment of the requirements for the degree of Doctor of Philosophy at the California Institute of Technology.

‡ Contribution No. 5192.

[1] F. I. Vilesov, B. L. Kurbatov, and A. N. Terenin, Dokl. Akad. Nauk SSSR **138,** 1329 (1961).
[2] D. W. Turner and M. I. Al-Joboury, J. Chem. Phys. **37,** 3007 (1962); D. W. Turner, C. Baker, A. D. Baker, and C. R. Brundle, *Molecular Photoelectron Spectroscopy* (Wiley, London, 1970).
[3] G. V. Marr, *Photoionization Processes in Gases* (Academic, New York, 1967), Chaps. 10–12.
[4] J. Cooper and R. N. Zare, J. Chem. Phys. **48,** 942 (1968); J. Cooper and R. N. Zare, in *Lectures in Theoretical Physics*, edited by S. Geltman, K. Mahanthappa, and N. Brittin (Gordon and Breach, New York, 1969), Vol. XI–C, p. 317.
[5] J. L. Hall and M. W. Siegel, J. Chem. Phys. **48,** 943 (1968).
[6] J. Berkowitz and H. Ehrhardt, Phys. Lett. **21,** 531 (1966); J. Berkowitz, H. Ehrhardt, and T. Tekaat, Z. Phys. **200,** 69 (1967).
[7] T. A. Carlson and A. E. Jonas, J. Chem. Phys. **55,** 4913 (1971).
[8] T. A. Carlson, G. E. McGuire, A. E. Jonas, K. L. Cheng, C. P. Anderson, C. C. Lu, and B. P. Pullen, in *Electron Spectroscopy*, edited by D. A. Shirley (North-Holland, Amsterdam, 1972), p. 207.
[9] P. Mitchell and K. Codling, Phys. Lett. **38A,** 31 (1972); M. J. Lynch, A. B. Gardner, and K. Codling, *ibid.* **40A,** 349 (1972).
[10] J. A. Kinsinger and J. W. Taylor, Int. J. Mass Spectrom. Ion Phys. **10,** 445 (1972).
[11] J. A. R. Samson, J. Opt. Soc. Am. **59,** 356 (1969).
[12] D. L. Ames, J. P. Maier, F. Watt, and D. W. Turner, Faraday Discuss. Chem. Soc. **54,** 277 (1972).
[13] J. A. R. Samson, Philos. Trans. R. Soc. Lond. A **268,** 141 (1970).
[14] J. W. McGowan, D. A. Vroom, and A. R. Comeaux, J. Chem. Phys. **51,** 5626 (1969); D. A. Vroom, A. R. Comeaux, and J. W. McGowan, Chem. Phys. Lett. **3,** 476 (1969).
[15] R. Morgenstern, A. Niehaus, and M. W. Ruf, Chem. Phys. Lett. **4,** 635 (1970); R. Morgenstern, A. Niehaus, and M. W. Ruf, in *Electronic and Atomic Collisions*, edited by L. Branscomb (North-Holland, Amsterdam, 1971), p. 167.
[16] H. Harrison, J. Chem. Phys. **52,** 901 (1970).
[17] J. L. Dehmer, W. A. Chupka, and J. Berkowitz, in *Electronic and Atomic Collisions*, edited by J. S. Risley and R. Geballe (University of Washington, Seattle, 1975), p. 565.
[18] D. C. Mason, A. Kuppermann, and D. M. Mintz, see Ref. 8, p. 269; D. M. Mintz and A. Kuppermann, see Ref. 17, p. 567.
[19] R. G. Houlgate, J. B. West, K. Codling, and G. V. Marr, J. Phys. B **7,** L470 (1974).
[20] W. S. Watson and D. T. Stewart, J. Phys. B **7,** L466 (1974).
[21] They cannot resolve the $^2P_{3/2} - {}^2P_{1/2}$ doublet of Ar split by 177 meV.
[22] R. G. Newburgh, L. Heroux, and H. E. Hinteregger, Appl. Opt. **1,** 733 (1962).
[23] J. A. R. Samson, *Techniques of Vacuum Ultraviolet Spectroscopy* (Wiley, New York, 1967), p. 231.
[24] G. L. Weissler, in *Handbuch der Physik*, edited by S. Flügge (Springer, Berlin, 1956), Bd. 21, p. 304.
[25] E. M. Purcell, Phys. Rev. **54,** 818 (1938).
[26] J. A. Simpson, Rev. Sci. Instrum. **35,** 1698 (1964).
[27] D. W. Turner, Proc. R. Soc. A **307,** 15 (1968).
[28] D. W. Turner, in *Chemical Spectroscopy and Photochemistry in the Vacuum-Ultraviolet*, edited by C. Sandorfy, P. J. Ausloos, and M. B. Robin (Reidel, Dordrecht, Holland, 1974), p. 25.
[29] A. H. Firester, Rev. Sci. Instrum. **37,** 1264 (1966).
[30] A. Savitzky and M. J. E. Golay, Anal. Chem. **36,** 1627 (1964).
[31] N. R. Draper and H. Smith, *Applied Regression Analysis* (Wiley, New York, 1966), Chap. 2.
[32] H. Margenau and G. M. Murphy, *The Mathematics of Physics and Chemistry* (Van Nostrand, New York, 1943), p. 498.
[33] D. J. Kennedy and S. T. Manson, Phys. Rev. A **5,** 227 (1972); and S. T. Manson (private communication).
[34] R. M. White, T. A. Carlson, and D. P. Spears, J. Electron Spectrosc. **3,** 59 (1974).
[35] J. C. Bünzli, A. J. Burak, and D. C. Frost, Tetrahedron **29,** 3735 (1973).

Downloaded 21 Dec 2005 to 131.215.225.171. Redistribution subject to AIP license or copyright, see http://rsi.aip.org/rsi/copyright.jsp